2012

Evaluation of Virtual Refrigerant Mass Flow Sensors

Woohyun Kim
kim644@purdue.edu

James E. Braun

Evaluation of Virtual Refrigerant Mass Flow Sensors

Woohyun Kim, James E. Braun*

Herrick Laboratory, Purdue University, Mechanical Engineering,
West Lafayette, IN, 47906, USA

* Corresponding Author: jbraun@purdue.edu

ABSTRACT

Refrigerant mass flow rate is an important measurement for monitoring equipment performance and enabling fault detection and diagnostics. However, a traditional mass flow meter is expensive to purchase and install. A virtual refrigerant mass flow sensor (VRMF) uses a mathematical model to estimate flow rate using low-cost measurements and can potentially be implemented at low cost. This study evaluates three VRMFs for estimating refrigerant mass flow rate. The first model uses a compressor map that relates refrigerant flow rate to measurements of inlet and outlet pressure, and inlet temperature measurements. The second model uses an energy-balance method on the compressor that uses a compressor map for power consumption, which is relatively independent of compressor faults that influence mass flow rate. The third model is developed using an empirical correlation for an electronic expansion valve (EEV) based on an orifice equation. The three VRMFs are shown to work well in estimating refrigerant mass flow rate for various systems under fault-free conditions with less than 5% RMS error. Each of the three mass flow rate estimates can be utilized to diagnose and track the following faults: 1) loss of compressor performance, 2) fouled condenser or evaporator filter, 3) faulty expansion device, respectively. For example, a compressor refrigerant flow map model only provides an accurate estimation when the compressor operates normally. When a compressor suction or discharge valve is leaking and the compressor is not delivering the expected flow, the energy-balance or EEV model can provide accurate flow estimates. In this case, the flow differences provide an indication of loss of compressor performance and can be used for fault detection and diagnostics, as will be demonstrated in this paper.

1. Introduction

Space heating, ventilation and air conditioning (HVAC) account for 40% of residential primary energy use, and for 30% of primary energy use in commercial buildings (DOE,2010). Over half of all conditioned floor space in the U.S. incorporates packaged HVAC equipment in their system design (Brodrick, 2000). The study conducted by Messenger (2008) indicates unitary air conditioners typically do not achieve rated efficiency because of improper installation or lack of servicing in the field. This paper suggested that service and replacement programs can yield energy savings on the order of 30 to 50%. The other study from ADM (2009) evaluated 109 units in the field and found that 89 had fault conditions, with 31having two or more faults. The average EER for the units increased from 6.6 before servicing to 7.0 after servicing, an average increase of 6.1%. Another investigation (Katipamula, 2005) suggested that faults or non-optimal control can cause the malfunction of equipment or performance degradation from 15 to 50%. Automated diagnostics has the potential to address these field performance problems and produce significant energy savings.

Refrigerant mass flow rate is an important measurement for monitoring HVAC systems and enabling Automated Fault Detection and Diagnostics (AFDD) to save energy and extend equipment life. Three different virtual refrigerant mass flow (VRMF) sensors were developed and evaluated in this study that use mathematical models to estimate flow rate using low cost measurements. The three approaches use: 1) a compressor map for refrigerant mass flow rate that uses inlet pressure and temperature and outlet pressure as inputs; 2) an energy-balance method employs a virtual sensor for power consumption based on a compressor map; 3) semi-empirical correlations for EEV and thermostatic expansion valves (TXV) that are based on an orifice equation. The models were trained and tested using data obtained from earlier laboratory studies. The application of the virtual sensors for diagnosing compressor valve faults and insensitivity to other faults are also demonstrated using the available data.

2. System descriptions and test conditions

Laboratory test data from a variety of sources were used to develop and evaluate VRMF sensors. Table 1 gives specifications for equipment where data were obtained through laboratory testing. The systems include a water-to-water heat pump with a variable-speed compressor, a residential air split system, and light commercial packaged systems with fixed and variable-speed compressors. The systems used either a TXV or EEV as an expansion device and R-22 or R-410A as a refrigerant. Some of the units included low-side accumulators.

Table 2 presents the range of operating test conditions for each unit, including the range of refrigerant flow rates encountered. The laboratory test data were obtained with variations in both indoor and ambient temperature. Three of four systems were tested with different condenser and evaporator airflow rates, which could represent faults associated with a dirty air filter or coil fouling. All of the systems except for system II were tested at different refrigerant charge levels to simulate improper charge service and refrigerant leakage. Systems I and III included simulated compressor valve leakage faults where a portion of the discharge flow from the compressor was bypassed to the compressor suction. System II was a laboratory setup for testing electronic expansion valves over a very wide range of refrigerant flows. Two different valves (B0B and B1F in the Table 1) were tested with two different refrigerants (R-410A and R-404A in Table 2). The B1F valve has a rated refrigerant flow (also cooling capacity and associated air/water flow) that is three times higher than that for the B0B valve with a 10 bar pressure difference across the maximum valve opening, based on the specification in the manufacturer's catalog. During the course of testing for system II, it was discovered that the compressor was not operating normally and was delivering significantly less than the rated flow. Thus, this data set could also be used to represent faulty compressor behavior. System III also included fault testing for a liquid line restriction (additional pressure drop increase through liquid line) and the presence of non-condensable gas (injection of nitrogen gas into the system). In general, only normal operating (i.e., no-fault) data were used to learn parameters of the VRMF sensors, whereas all of the data were used for assessing VRMF sensor performance.

Table 1 System descriptions for laboratory test data

System		Size (kW)	Refrigerant	Compressor	Expansion Device	Accumulator	System Type
I	(Kim,2005)	3	R-22	Variable-speed compressor	EEV	No	Water to Water
II	(Bach, 2010)	7.0	R-410A R-404A	Fixed-speed compressors	EEV (B0B/B1F)	Yes	
III	(Payne, 2008)	8.8	R-410A		TXV	Yes	Air Split Type

Table 2 Test conditions for laboratory testing data

System	Indoor Temperature		Ambient temperature	Percentage of rate refrigerant mass flow rate	Indoor air/ water flow rate	Outdoor air/ water flow rate	Refrigerant charge
	Dry	Wet					
	(C)	(C)	(F)	[%]	[%]	[%]	[%]
I	26.7	-	15/24/32/40	65~100	35~100	25~100	60~100
II	26.7	-	35 / 28	20~100 (R410A) 10~100 (R404A)	100	100	100
III	26.7 / 21	19 / 15/ Dry	28/ 35/ 39	60~100	70~100	50~100 (Coil Block)	70~130

3. VRMF sensor I based on a compressor flow map

3.1 Development of VRMF sensor I

A compressor map is used to estimate refrigerant mass flow rate using input measurements of inlet and outlet pressure. Based on ARI Standard 540, refrigerant mass flow rate for a fixed speed compressor can be represented using a 10-coefficient polynomial equation for a specified amount of superheat. The map at the specified superheat is typically corrected using the ratio of the compressor suction density at the actual superheat to the density at the

tested superheat. Based on the ARI model form, the VRMF Sensor I for a fixed-speed compressor is determined using equation 1.

$$\dot{m}_{map} = \rho_{suc} \cdot \left(a_0 + a_1 T_c + a_2 T_c + a_3 T_e^2 + a_4 T_e^2 + a_5 T_c \cdot T_c + a_6 T_e^3 + a_7 T_e^3 + a_8 T_e^2 \cdot T_c + a_9 T_c^2 \cdot T_e\right) \quad (1)$$

where m_{map} is the estimated refrigerant mass flow rate, the a's are empirical coefficients, T_e is evaporating saturation temperature, T_c is condensing saturation temperature, and ρ_{suc} is the density at the suction (inlet) of the compressor.

The development of VRMF sensor I for a variable-speed compressor is explained in Kim and Braun (2012). Equation 1 is used to map the mass flow rate for a rated frequency and this is corrected for other frequencies using a second-order polynomial as given in equation 2. The c and b coefficients are estimated using regression analysis applied to experimental data.

$$\dot{m}_{map} = \rho_{suc} \cdot \left(c_1 (f - f_{rated})^2 + c_2 (f - f_{rated}) + c_3\right) \cdot \left(b_0 + b_1 T_c + b_2 T_c + b_3 T_e^2 + b_4 T_e^2 + b_5 T_c \cdot T_c\right)_{rated,\, frequency} \quad (2)$$

where the b's and c's are empirical coefficients, f is compressor frequency, and f_{rated} is the rated compressor frequency.

3.2 Performance of VRMF sensor I

Figures 1 and 2 show the performance of VRMF Sensor I that is based on a compressor map. The terms "Normal", "Comp Fault", "Cond Fault", "Evap Fault", "Liquid Fault", "Charge Fault", and "NonCond Fault" stand for no fault, compressor leakage fault, condenser fouling fault, evaporator fouling fault, liquid-line restriction fault, refrigerant leakage fault, and non-condensable gas fault, respectively To evaluate performance of the VRMF sensor, the predicted ratio of refrigerant mass flow rate to rated flow is compared to the value determined using measurements. The VRMF models were developed using only the normal data but used to predict flow rates for all of the fault tests.

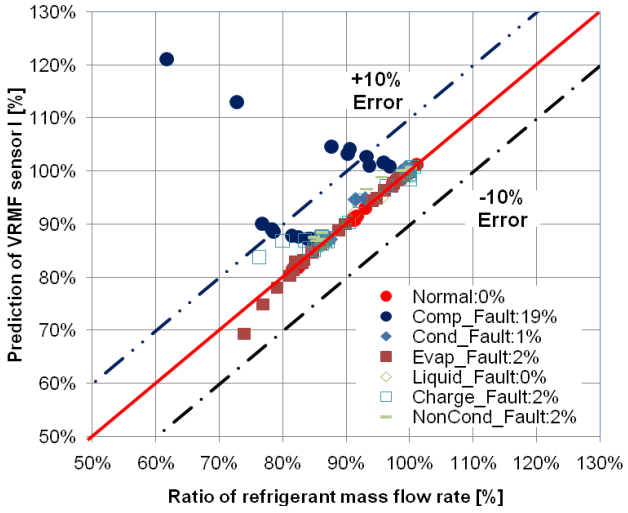

Figure 1: Performance of VRMF sensor based on fixed-speed compressor map for system III under no fault and fault conditions (RMS of sensor errors shown for each fault type)

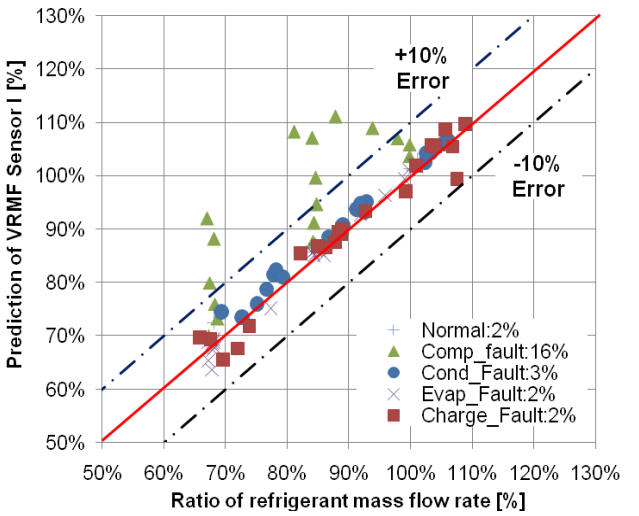

Figure 2: Performance of VRMF sensor based on variable speed compressor map for system I under no fault and fault conditions (RMS of sensor errors shown for each fault type)

Figure 1 shows the performance of VRMF sensor I for system III with a fixed-speed compressor under no fault and various faulty conditions. The RMS error is generally less than 2% for normal operation and with a variety of faults except for compressor valve leakage. For the range of compressor leakage conditions considered, the RMS error for the VRMF sensor I was 19%. In general, the error increases with the severity of the compressor leakage fault. As a result, differences between refrigerant flow determined using VRMF sensor I and other VRMF sensors can be used to diagnose a fault associated with the compressor not delivering the proper refrigerant flow.

Figure 2 shows the performance of VRMF sensor I for system I with a variable-speed compressor under no fault and various fault conditions. Although the VRMF sensor I was trained using only no-fault data, it accurately estimates mass flow rate for faulty conditions over the range of operating frequencies, except for the compressor valve leakage fault. The RMS errors for VRMF sensor I were less than 3% for condenser fouling, refrigerant charge, and evaporator fouling conditions, respectively. However, VRMF sensor I predictions were about 16% higher than measurements for the range of compressor fault conditions considered, with the errors increasing with fault level.

4. VRMF sensor II based on a compressor energy balance

4.1 Development of VRMF sensor II

In order to diagnose compressor flow problems, it is necessary to have an alternative VRMF sensor. One alternative approach is to use an energy balance on the compressor to estimate flow rate as shown in equation 3. Li (2006) demonstrated that this method provides accurate flow predictions when using a virtual compressor sensor for power consumption, even in the presence of a compressor valve leakage fault or other faults. Compared to the map-based method, the energy balance model is much simpler and can be used for both fixed-speed and variable-speed compressors.

$$\dot{m}_{energy} = \frac{\dot{W} \cdot (1 - \alpha_{loss})}{h_{dis}(T_{dis}, P_{dis}) - h_{suc}(T_{suc}, P_{suc})} \tag{3}$$

where α_{loss} is compressor heat loss ratio, W is compressor power consumption, and $h_{dis}(T_{dis},P_{dis})$ and $h_{suc}(T_{suc},P_{suc})$ are the discharge line and suction line refrigerant enthalpy. The compressor power consumption, discharge pressure (P_{dis}) and suction pressure (P_{suc}) can be estimated using other virtual sensors.

α_{loss} is generally very small (under 5%) for equipment having a fixed-speed compressor operating normally. However, it can be more significant at low compressor speeds for variable-speed equipment or with faults for fixed-speed equipment. For example, decreasing the compressor frequency from 60Hz to 30Hz almost doubles the heat loss as a fraction of the power input. To provide more accurate mass flow rates predictions under various faulty conditions and/or speeds, an empirical model for α_{loss} was developed that is trained using regression applied to data. The model for fixed-speed equipment is given in equation 4, while a function for variable-speed equipment is shown in equation 5.

$$\alpha_{loss,pred} = c_0 + c_1 P_{dis} + c_2 P_{suc} + c_3 T_{dis} + c_4 T_{suc} \tag{4}$$

$$\alpha_{loss,pred} = c_0 + c_1 P_{dis} + c_2 P_{suc} + c_3 T_{dis} + c_4 T_{suc} + c_5 f \tag{5}$$

where the c's are empirical coefficients, P_{suc} is suction pressure, P_{dis} is discharge pressure, T_{amb} is compressor ambient temperature, T_{suc} is suction temperature, and f is speed of the compressor motor.

4.2 Performance of VRMF sensor II

Figure 3 shows the performance of VRMF sensor II for system III with a fixed-speed compressor. The mass flow rate prediction was determined using heat loss estimates and predictions of other virtual sensors. The heat loss model was determined using data for normal operation where the heat loss was determined from an energy balance on the compressor with the flow measured. The power consumption was determined using a map in terms of suction pressure and temperature and discharge pressure as outlined in Kim and Braun (2012). The RMS error for the VRMF sensor was less than 3% for all of the data, including both normal and faulty conditions. The larger errors for the evaporator fouling occurred when the superheat at the compressor inlet was below 1.5F. The incorrect compressor suction enthalpy due to a two-phase refrigerant inlet state led to the inaccurate estimate of mass flow rate. The VRMF sensor II is relatively independent of compressor faults compared to the VRMF sensor I.

Figure 4 shows the performance of VRMF sensor II for system II with a variable-speed compressor. The mass flow rate estimates were compared to measurements for a range of different faults at different fault levels. The RMS error for the VRMF sensor II is less than 5%. Except for several low compressor speed conditions, the VRMF works well regardless of the fault conditions. However, there were some significant errors (10%) at low frequencies. Additional

work is necessary to accurately determine heat loss for variable-speed compressors when operating at low frequencies.

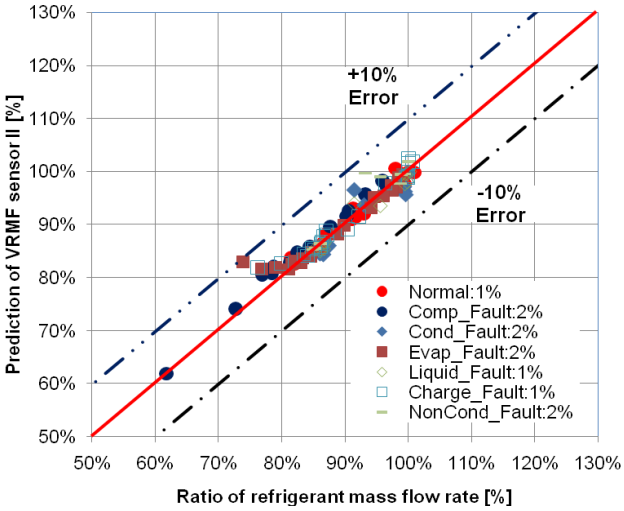

Figure 3: Performance of VRMF sensor II based on energy balance for system III under no fault and fault conditions (RMS of errors shown for each fault type)

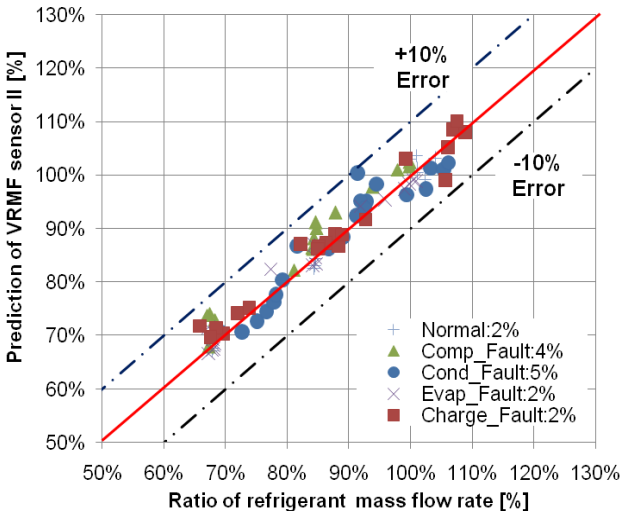

Figure 4: Performance of VRMF sensor II based on energy balance for system I under no fault and fault conditions (RMS of errors shown for each fault type)

5. VRMF sensor III based on an expansion valve model

Expansion devices are used to drop the pressure of the refrigerant and to regulate the refrigerant mass flow rate in response to a variable load. There are three types of expansion devices used in air conditioners: fixed-orifice (FXO), thermostatic expansion valve (TXV), and electronic expansion valve (EEV). Even though an FXO has advantages of simplicity and low cost, it is not appropriate for a system that requires precise flow control for a wide range of flow rate requirements. TXV and EEV devices are adjustable throat-area expansion valves. The TXV adopts a mechanical control method to obtain relatively constant superheat at the evaporator outlet. The EEV provides a more precise control of superheat and fast flow control for a wide range of mass flow rates because it uses electronic actuation and sensor information along with a digital feedback controller. Most of the previous literature on modeling of expansion devices has focused on constant-area expansion devices, such as FXO. Models for predicting the mass flow characteristics of TXVs and EEVs are limited. Li (2008) developed generalized expressions for TXV mass flow as a function of superheat and valve. Shanwei et al. (2005) and Park et al. (2007) developed empirical correlations for mass flow rate through an EEV by performing the dimensionless analysis based on a power law form. However, these existing models require either detailed geometric parameters or many measurements to represent performance. This paper presents VRMF sensors for TXV and EEV devices based on a semi-empirical model that can be trained using a relatively small amount of data and then can estimate refrigerant mass flow rate as part of an automated diagnostic system.

5.1 Development of VRMF sensor III for TXV

The valve opening for a TXV is determined by a force balance on a diaphragm, as depicted in Figure 5. The bulb and suction-line pressure act on opposite sides of the diaphragm and coupled with the spring force, control the effective orifice area. The evaporator inlet and condenser pressure influence the flow rate through the orifice for a given opening. The bulb typically contains a two-phase mixture of the same refrigerant that is employed within the system. Therefore, when a positive superheat exists at the evaporator outlet then there is a positive difference between the bulb and evaporator outlet pressures acting the diaphragm. The spring is used to ensure a positive superheat at the evaporator exit since the bulb pressure must be greater than the evaporator exit pressure in order to overcome the force of the spring.

As depicted in Figure 5, a conical pin moves up and down to change the open area for refrigerant flow in response to the valve control. The mass flow rate through the TXV is assumed to be linear function of the open area as given in equation 6.

$$m_{TXV} = \left(\frac{A_{orifice} - A_{pin}}{A_{orifice}} \right) \cdot m_{\max} \tag{6}$$

where $A_{orifice}= ((D_{orifice})^2 \cdot \pi)/4$ is the area at the full opening, $A_{pin}= ((D_{pin})^2 \cdot \pi)/4$ is closed area associated with the pin, and m_{max} is the refrigerant mass flow rate associated with a full open condition.

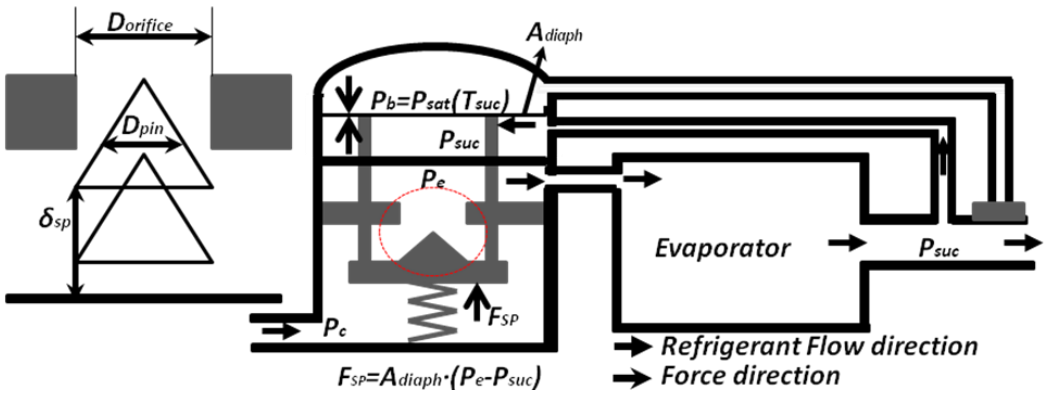

Figure 5: Diagram of TXV

The maximum flow rate for a given valve is a function of the pressure drop across the valve and the size of the orifice. The maximum flow rate for a given orifice is calculated using the empirical correlation given in equations 7 and 8, as developed by Hmjak (1989).

$$\dot{m}_{\max} = C_0 \cdot A_{orifice} \cdot \sqrt{\left(\left(2 \cdot \rho_f \left[P_c - P_e \cdot K\right]\right)\right)} = C_1 \cdot \sqrt{\left(2 \cdot \rho_f \left[P_c - P_e \cdot K\right]\right)} \tag{7}$$

$$K = C_2 \cdot \left(\frac{SC + 2}{T_{Cri}} \right)^{C_3} + C_4 \left(\frac{P_{cri} - P_e}{P_{cri}} \right) + C_5 \tag{8}$$

where the C's are empirical coefficients, $(P_c\text{-}P_e)$ is the difference between the valve inlet pressure and the evaporating pressure, ρ_f is the density of the refrigerant at the valve inlet, SC is the subcooling of the refrigerant at the valve inlet, T_{cri} and P_{cri} are the critical temperature and pressure.

The spring deflection, δ_{sp} needs to known in order to find the effective orifice area. The deflection of the spring can be found using equation 9.

$$\delta_{sp} = \frac{F_{sp} - F_{sp,cl}}{k_{sp}} \tag{9}$$

where F_{sp} is the spring force, $F_{sp,cl}$ is the spring force when the valve is closed and k_{sp} is the spring constant. Both $F_{sp,cl}$ and k_{sp} are fixed for a given expansion valve. F_{sp} is calculated from a quasi-static force balance on the diaphragm, as shown in equation 10.

$$F_{sp} = A_{diaph} \cdot \left(P_b - P_{suc}\right) = A_{diaph} \cdot \left(P_e - P_{suc}\right) \tag{10}$$

where $(P_b\text{-}P_{suc})$ is the pressure difference between bulb and suction line, and A_{diaph} is the area of diaphragm. $F_{sp,cl}$, A_{diaph} and k_{sp} are constants based on the valve design and initial setting.

Since the spring force is a linear function of the deflection, the spring deflection can be expressed using empirical coefficients *a*'s, as shown in equation 11.

$$\delta_{sp} = \frac{A_{diaph} \cdot (P_e - P_{suc}) - F_{sp,cl}}{k_{sp}} = a_1 (P_e - P_{suc}) + a_2 \tag{11}$$

If the pin deflection is zero, no refrigerant flows through the orifice, and if the pin deflection is at some maximum value, the pin will not obstruct the flow and the valve will operate at the maximum flow rate. The effective orifice area is calculated by subtracting the obstructing area of the pin from the area of the valve orifice. The VRMF sensor for a TXV is developed by substituting δ_{sp} from equation 11 into equation 6 and expressing the result in terms of new empirical coefficients that are determined through regression.

$$\dot{m}_{TXV} = \left(\frac{A_{orifice} - A_{pin}}{A_{orifice}} \right) \cdot \dot{m}_{\max} = \frac{\pi}{4} \left(\delta_{\max}^2 - \delta_{sp}^2 \right) \cdot \dot{m}_{\max} = \frac{\pi}{4} \left(C_2 - \delta_{sp}^2 \right) \cdot \dot{m}_{\max}$$
$$= \left(a_3 (P_e - P_{suc})^2 + a_4 (P_e - P_{suc}) + a_5 \right) \cdot \dot{m}_{\max} \tag{12}$$

5.2 Performance of VRMF sensor III for TXV

The empirical coefficients C_1, C_2, C_3, C_4 and C_5 within orifice equations 7 and 8 were estimated by minimizing mass flow rate prediction errors using fully open TXV test data and non-linear regression. Fully open TXV test data were collected from the conditions where superheat of the compressor inlet was higher than the rated superheat. The empirical coefficients a_3, a_4, and a_5 within the TXV model equation 12 were estimated based on the available normal test data with superheat under control using linear regression. The data includes variations in ambient temperature, and indoor dry bulb temperature with positive subcooling entering the valve. Since equation 8 uses subcooling as an input, zero subcooling data were disregarded for training and testing. The parameter estimation methods minimized the errors between predicted and known mass flow rates. The resulting model with empirical coefficients determined from normal data was applied to predict refrigerant mass flow rate for all of the available data including various fault conditions.

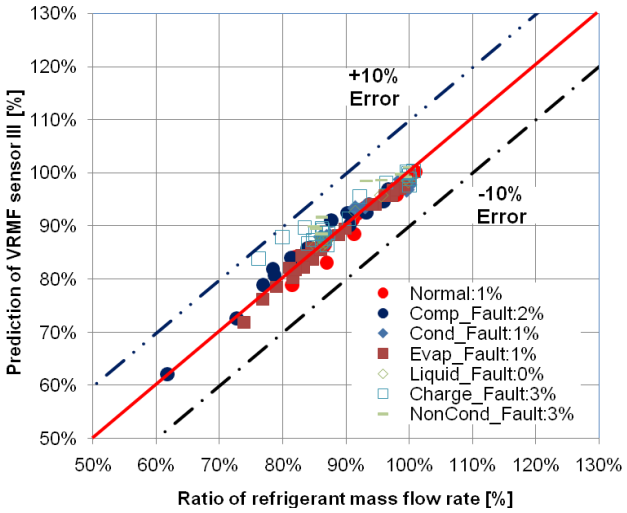

Figure 6: Performance of VRMF sensor III based on TXV for system III under no fault and fault conditions (RMS of sensor errors shown for each fault type)

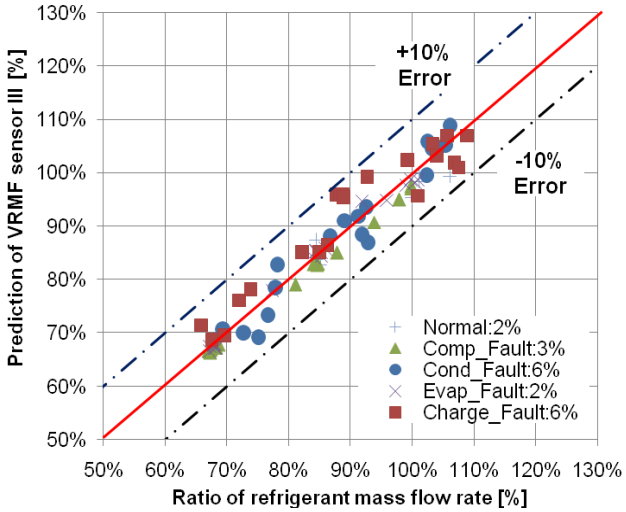

Figure 7: Performance of VRMF sensor III based on EEV for system I under no fault and fault conditions (RMS of sensor errors shown for each fault type)

Figure 6 shows refrigerant mass flow rate estimated from the VRMF sensor III for TXV applied to system III with six different kinds of faults individually implemented. The overall RMS errors were about 1% for no fault conditions and 3% of actual mass flow rate for all fault conditions. The performance of the VRMF sensor is very good over a wide range of refrigerant mass flow rates and operating conditions regardless of the fault. There were some significant errors of about 10% for low refrigerant charge levels when the entering subcooling was almost zero. With zero subcooling and two-phase conditions entering the TXV, the VRMF sensor III may not be reliable.

5.3 Development of VRMF sensor III for EEV

Electronic expansion valves (EEV) were developed in the 1980s to provide tighter and more stable control of superheat with faster response. The applications of EEV for high efficiency air conditioner and multi-evaporator heat pump systems have increased in recent years. However, mass flow models of EEV for fault detection and diagnosis are very limited. In this study, the VRMF sensor based on an empirical correlation can predict refrigerant mass flow rates through EEV.

The empirical mass flow correlation was developed by incorporating a dimensionless coefficient in terms of EEV geometries and operating conditions into the orifice equations 6 and 7 because the only difference between the EEV and TXV model is how the area opens and closes. The empirical correlation for VRMF sensor is given in equation 13. The variation of the actual orifice diameter controls the refrigerant flow area for flow restriction. The mass flow rate proportionally increases with the rise of the flow area.

$$\dot{m}_{EEV} = A_{actual} \cdot \dot{m}_{\max} = \left(\frac{\pi \cdot D_{acutal}^2}{4} \right) \cdot C_1 \cdot \sqrt{\left(2 \cdot \rho_f \left[P_c - P_e \cdot \left(C_2 \cdot \left(\frac{SC+2}{T_{Cri}} \right)^{C_3} + C_4 \left(\frac{P_{cri} - P_e}{P_{cri}} \right) + C_5 \right) \right] \right)} \tag{13}$$

where the *C's* are empirical coefficients, D_{actual} is actual orifice diameter (see Figure 8), ρ_f is the density of refrigerant at the valve inlet, P_c and P_e are the inlet pressure and evaporator pressure.

Figure 8 shows the flow passage structure and geometric representation for an EEV. A needle valve moves up and down to change the flow area, typically using a stepper motor to maintain precise control of the refrigerant superheat at the evaporator exit. At a certain pin tip position *h*, the refrigerant flow area A_{actual} can be calculated by subtracting the obstructing area of the needle from the area of the valve orifice as developed by Li (2008) and given in equation 14.

$$A_{actual} = \frac{\pi \cdot D_{actual}^2}{4} = \frac{\pi}{4} \left(D_{orifice}^2 - D_{pin}^2 \right) = \frac{\pi}{4} \left(D_{orifice}^2 - \left(2 \cdot \tan\theta \cdot (H-h) \right)^2 \right) \tag{14}$$

where $D_{pin}=(2 \cdot tan\theta \cdot (H-h))$ is the current needle diameter that is within the plane of the flow orifice, and $D_{orifice}=2 \cdot H \cdot tan\theta$ is the orifice diameter. The current needle diameter can then be expressed in terms of the orifice diameter and needle position as shown in equation 15.

$$D_{pin} = \left(2 \cdot \frac{D_{orifice}}{2 \cdot H} \cdot (H-h) \right) = D_{orifice} \left(1 - \frac{h}{H} \right) \tag{15}$$

Equations 14 and 15 can be combined to express the refrigerant flow area for any needle position, A_{actual}, as

$$A_{actual} = \frac{\pi}{4} \left(D_{orifice}^2 - D_{orifice}^2 \left(1 - \frac{2 \cdot h}{H} + \left(\frac{h}{H} \right)^2 \right) \right) = \frac{\pi}{4} \cdot D_{orifice}^2 \cdot \frac{h}{H} \cdot \left(2 - \frac{h}{H} \right) \tag{16}$$

The refrigerant mass flow rate through the EEV can be obtained by substituting the refrigerant flow area, equation 16, into the general model equation 13.

$$\dot{m}_{EEV} = C_1 \cdot \left(\frac{\pi \cdot D_{orifice}^2}{4} \right) \cdot \left(\frac{h}{H} \right) \cdot \left(2 - \frac{h}{H} \right) \sqrt{\left(2 \cdot \rho_f \left[P_c - P_e \cdot K \right] \right)} \tag{17}$$

The flow area of the EEV varies with the up-and-down movement of the needle valve that is driven by a step motor. The needle position (h) is linearly proportional to the motor step of EEV, as given in equation 18.

$$h = \frac{EEVSTEP_{current}}{EEVSTEP_{\max}} \cdot H \tag{18}$$

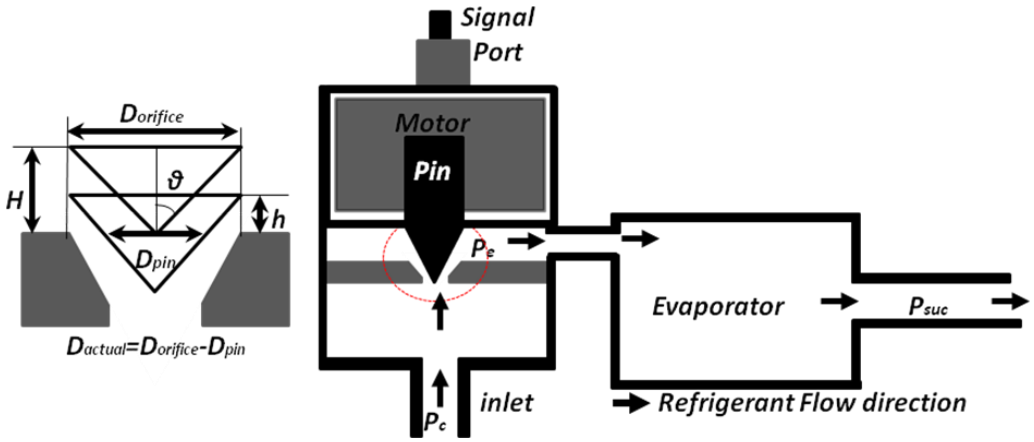

Figure 8: Flow passage structure and geometric models for EEV

In this study, the VRMF sensor for an EEV was developed by substituting the ratio of motor step, equation 18, into the EEV refrigerant mass flow rate equation 17. The correction coefficient in 19 can be determined using linear regression based on normal test data.

$$\dot{m}_{EEV} = \left(\frac{EEVSTEP_{current}}{EEVSTEP_{\max}}\right)\cdot\left(C_2 - C_3\cdot\frac{EEVSTEP_{current}}{EEVSTEP_{\max}}\right)\cdot\left(\frac{\pi\cdot D_{orifice}^2}{4}\right)\cdot\sqrt{\left(2\cdot\rho_f\left[P_c - P_e\cdot K\right]\right)} \tag{19}$$

5.4 Performance of the VRMF sensor III for EEV

The empirical coefficients within orifice equation 8 were determined using non-linear regression applied to fully open EEV data. Fully open EEV data were collected from the conditions where the motor step was at a maximum. Like the TXV, equation 8 uses subcooling as in input, and thus zero subcooling data were disregarded for training and testing. Once the empirical coefficients of orifice equation are obtained, the EEV equation 19 was then fit to normal operating (i.e., no-fault) data using linear regression. The best fit equation was then used to predict the refrigerant mass flow rate through the EEV for all available test data including various fault conditions.

Figure 7 shows performance of the VRMF sensor III for EEV approach applied to system I. The model provides results that are generally within 6% over a wide range of mass flow rates and operating conditions. Larger errors for low refrigerant charge and condenser fouling occurred when the subcooling at the condenser outlet was below 2F.

Figures 9 and 10 show performance of the VRMF sensor III for EEV applied to system II with R-410A and R-404A as refrigerant. Results are presented for two different EEVs that were tested in this system. Overall, the RMS errors of the VRMF sensor III were 6% and 5% for R-410A and R-404A, respectively. Some of the larger errors may be associated with two-phase refrigerant conditions at the EEV inlet with near-zero subcooling.

6. Application of VRMF sensors for fault detection and diagnosis

Outputs from the three VRMF sensors can be compared in order to detect a fault and localize faults within a system, including: 1) loss of compressor performance, 2) faulty compressor motor, and 3) faulty expansion device. Figures 11 to 14 demonstrate the use of the VRMF sensors for isolating a fault condition where the compressor is not providing expected flow.

Figure 11 shows comparisons of the three VRMF sensors with mass flow measurements for system III operating at fixed speed with a simulated compressor valve leakage fault. With this fault, the refrigerant mass flow rate is reduced compared to normal operation. As a result, the compressor map over-predicts refrigerant mass flow rate whereas the other VRMF sensors provide accurate flow estimates. The RMS errors for compressor energy balance

model and TXV models were about 2 %, whereas the RMS error for the fixed-speed compressor model was 19 %. Thus, a compressor flow fault could be isolated through comparison of the VRMF sensors for this case.

Figure 12 similar results for system I having a variable-speed compressor and EEV. The RMS errors for the VRMF sensors were about 5 % based on a compressor energy balance and 3 % based on the EEV model, but were approximately 16 % for the variable-speed compressor map.

Figures 13 and 14 show results for system II with B1F and B0B as expansion devices and the two different refrigerant types, R-410A and R-404a. The data did not include information that could be used to evaluate the energy balance method. The tests covered a wide range of compressor fault levels from 10 to 100%. For either set of test data, a compressor fault could be readily identified by comparing predictions of the compressor map with those from the EEV model.

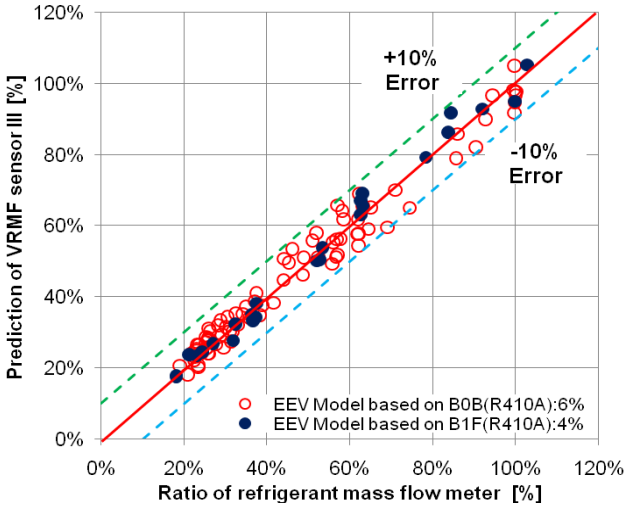

Figure 9: Performance of VRMF sensor III based on EEV with R410a as refrigerant for system II

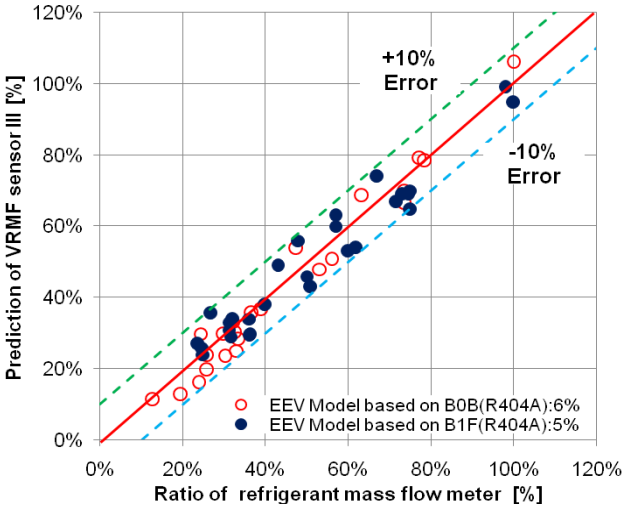

Figure 10: Performance of VRMF sensor III based on EEV with R410a as refrigerant for system II

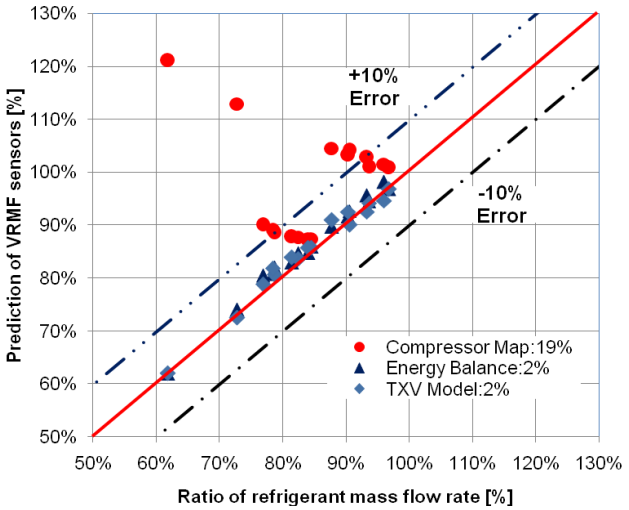

Figure 11: Comparison of VRMF sensor outputs for system III with compressor flow fault

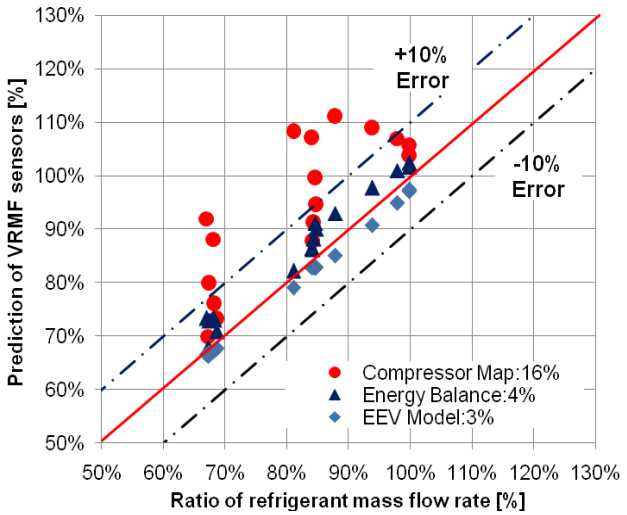

Figure 12: Comparison of VRMF sensor outputs for system I with compressor flow fault

7. CONCLUSIONS

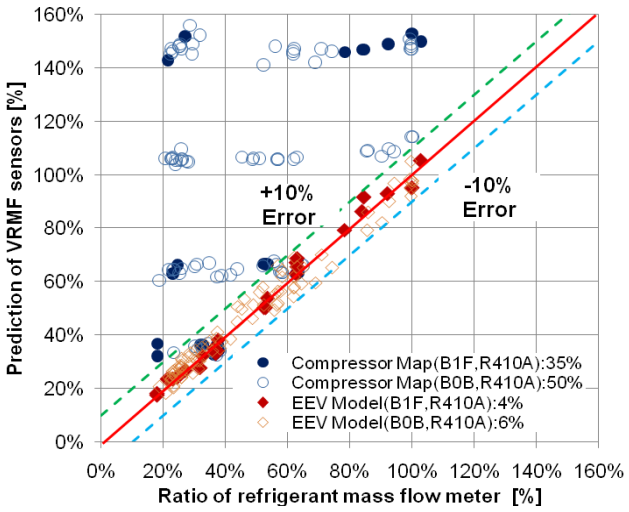

Figure 13: Comparison of VRMF sensor outputs for system II (R410A) with compressor flow fault

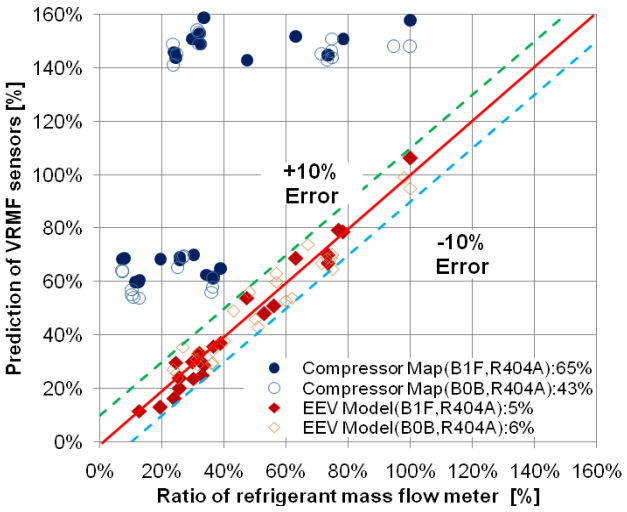

Figure 14: Comparison of VRMF sensor outputs for system II (R404A) with compressor flow fault

Refrigerant mass flow rate is an important measurement for equipment performance monitoring, fault detection, and diagnostics. However, a typical refrigerant mass flow meter is expensive and installation for existing field equipment is complicated because it requires an equipment modification that can lead to refrigerant leakage. To enable low-cost implementations for on-line performance monitoring and automated diagnostics, three different virtual refrigerant mass flow (VRMF) sensors were developed for estimating refrigerant mass flow rate from low-cost measurements that are based on: 1) a compressor map, 2) a compressor energy balance, and 3) a semi-empirical correlation for the expansion device (TXV or EEV).

The VRMF sensors presented in this paper were validated for systems having fixed and variable-speed compressors, different refrigerants, and different expansion devices (TXV/EXV) operating over a wide range of operating conditions both with and without faults. The three VRMFs work well in estimating the refrigerant mass flow rate for the various systems under fault-free conditions with less than a 5% RMS error. Predictions from the VRMF sensor based on a compressor map deviate from the other VRMF sensors in the presence of a compressor fault with the deviations growing with the magnitude of the fault. These differences can be used within a diagnostic system to isolate this particular fault since the accuracy of the energy balance model and expansion device models are independent of compressor flow faults.

NOMENCLATURE

A	area	m^2	**Subscripts**	
a, b, c	Empirical constants		*actual*	Actual
$C_{d,eev}$	Correction coefficient for EEV model		*b*	Bulb
$C_{d,eev,pi}$	Correction coefficient for PI theorem		*c*	Condenser
D	Diameter	m	*cri*	Critical
d	Current needle diameter	m	*diaph*	Diagram
EEV	Electronic expansion valve		*dis*	Discharge
EEVSTEP	Opening of EEV	Step	*e*	Evaporator
F	Force	N	*dis*	Discharge
f	Compressor speed	Hz	*f*	Liquid
FDD	Fault Detection and Diagnostics		*g*	Gas
H	Maximum needle position	m	*max*	Maximum

h	Certain needle position	m	*orifice*	Orifice
h	Enthalpy	kJ/kg	*Rated*	Rated condition
k_{sp}	Spring constant	N/m	*sp*	Spring
$\dot{m}_{map}$	Refrigerant mass flow rate based on compressor map	kg/s	*sp,cl*	Closed spring
$\dot{m}_{energy}$	Refrigerant mass flow rate based on compressor energy balance	kg/s	*suc*	Suction
$\dot{m}_{TXV}$	Refrigerant mass flow rate based on TXV model	kg/s	*TXV*	Thermostatic valve expansion
$\dot{m}_{EEV}$	Refrigerant mass flow rate based on EEV model	kg/s		
P	Pressure	Pa		**Greek**
$\dot{W}$	Compressor input Power	W	ρ	Desnsity
SC	Subcooling	C	α_{loss}	Compressor heat loss ratio
TXV	Thermostatic valve expansion		δ_{sp}	Spring deflection
T	Temperature	C	μ	Viscosity
VRMF	Virtual refrigerant mass flow sensor		θ	Angle of pin

REFERENCES

ADM Associates, 2009, Market assessment and field M&V study for comprehensive packaged A/C systems program, SCE0286, July24, 2009.

American Refrigeration Institute (ARI), 1999, Positive displacement refrigerant compressors and compressor units.

Bach, C. 2010, Personal communication, Ray W. Herrick Laboratories, Purdue University.

Brodrick, J., 2000, Are fans blowing your energy budget?, *HPAC Heating/Piping/Air Conditioning Engineering*, p. 74-77.

Hrnjak, P.S., Lenger, M.J., and Jacobi, A.M., 1998, Superheat stability of an evaporator and thermostatic expansion valve, air conditioning and refrigeration center., University of Illinois at Urbana-Champaign

Katipamula, S. and Brambley, M.R., 2005. Methods for fault detection, diagnostics, and prognostics for vapor compression equipment Systems, A Review, Part I, *HVAR&R Research*, Vol. 11(1), p. 3-25.

Kim, M. and Kim, M.S., 2003, Performance investigation of a variable speed vapor compression system for fault detection and diagnosis, *International Journal of Refrigerant*, Vol. 28, p. 481-488.

Kim, W.H and Braun, J.E., 2012, Virtual refrigerant mass flow and power sensors for variable-speed compressors, *International Refrigerant and Air conditioning Conference*, No. 2299.

Li, H. and Braun, J.E., 2008, A method for modeling adjustable throat-area expansion valves using manufacturers' rating data, *HVAC&R Research*, Vol. 14(4), p. 581-598.

Messenger, M., Strategic Plan to Reduce the Energy Impact of Air Conditioners, CEC-400-2008-010, June, 2008.

Payne, W. V., Kim, M. S., Yoon, S. H., and Domanski, P. A., 2008, Cooling mode fault detection and diagnosis method for a residential Heat Pump., NIST SP 1087; NIST Special Publication p.1087; 98

Park, C., Cho, H. and Kim, Y., 2007, Mass flow characteristics and empirical modeling of R22 AND R410A flowing through electronic expansion valves, *International Journal of Refrigeration*, Vol. 03, p. 1-7.

Shanwei, M., Chuan, Z., Jiangping, C., and Zhiujiu, C., 2005, Experimental research on refrigerant mass flow coefficient of electronic expansion valve, *Applied Thermal Eng.*, Vol. 25, p. 2351-2366.

U.S. Department of Energy, 2010, Energy efficiency trends in residential and commercial buildings, August, 2010.

ACKNOWLEDGEMENT

This work was supported by the Department of Energy through the Energy Efficient Buildings Hub.